CrossMark click for updates

Fetal endocannabinoids orchestrate the organization of pancreatic islet microarchitecture

Katarzyna Malenczyk[a,b,c], Erik Keimpema[a,c], Fabiana Piscitelli[d], Daniela Calvigioni[a], Peyman Björklund[e], Kenneth Mackie[f], Vincenzo Di Marzo[d], Tomas G. M. Hökfelt[g,1], Agnieszka Dobrzyn[b], and Tibor Harkany[a,c,1]

[a]Division of Molecular Neurobiology, Department of Medical Biochemistry & Biophysics, Karolinska Institutet, SE-17177 Stockholm, Sweden; [b]Nencki Institute of Experimental Biology, 02-093 Warsaw, Poland; [c]Department of Molecular Neurosciences, Center for Brain Research, Medical University of Vienna, A-1090 Vienna, Austria; [d]Endocannabinoid Research Group, Institute of Biomolecular Chemistry, National Research Council, I-80078 Pozzuoli, Naples, Italy; [e]Department of Surgical Sciences, Uppsala University, SE-75185 Uppsala, Sweden; [f]Department of Psychological and Brain Sciences, Gill Center for Neuroscience, Indiana University, Bloomington, IN 47405; and [g]Department of Neuroscience, Karolinska Institutet, SE-17177 Stockholm, Sweden

Contributed by Tomas G. M. Hökfelt, September 28, 2015 (sent for review June 4, 2015; reviewed by Leif Groop, Tamas L. Horvath, and George Kunos)

Endocannabinoids are implicated in the control of glucose utilization and energy homeostasis by orchestrating pancreatic hormone release. Moreover, in some cell niches, endocannabinoids regulate cell proliferation, fate determination, and migration. Nevertheless, endocannabinoid contributions to the development of the endocrine pancreas remain unknown. Here, we show that α cells produce the endocannabinoid 2-arachidonoylglycerol (2-AG) in mouse fetuses and human pancreatic islets, which primes the recruitment of β cells by CB_1 cannabinoid receptor (CB_1R) engagement. Using subtractive pharmacology, we extend these findings to anandamide, a promiscuous endocannabinoid/endovanilloid ligand, which impacts both the determination of islet size by cell proliferation and α/β cell sorting by differential activation of transient receptor potential cation channel subfamily V member 1 (TRPV1) and CB_1Rs. Accordingly, genetic disruption of TRPV1 channels increases islet size whereas CB_1R knockout augments cellular heterogeneity and favors insulin over glucagon release. Dietary enrichment in ω-3 fatty acids during pregnancy and lactation in mice, which permanently reduces endocannabinoid levels in the offspring, phenocopies $CB_1R^{-/-}$ islet microstructure and improves coordinated hormone secretion. Overall, our data mechanistically link endocannabinoids to cell proliferation and sorting during pancreatic islet formation, as well as to life-long programming of hormonal determinants of glucose homeostasis.

cell adhesion | diabetes | G protein-coupled receptor | migration | proliferation

Anandamide (AEA) and 2-arachydonoylglycerol (2-AG), major endocannabinoids (eCBs), are involved in the regulation of energy homeostasis through coordinated actions in peripheral organs (adipose tissue, liver, and pancreas) and brain (hypothalamus, ventral striatum) (1). eCB signals are particularly significant to coordinate the regulated release of insulin and glucagon from mature pancreatic islets (2–6). Genetic evidence from CB_1 cannabinoid receptor$^{-/-}$ ($CB_1R^{-/-}$) mice supports these findings because $CB_1R^{-/-}$ mice are lean, resistant to high fat diet-induced obesity and diabetes (4, 7–9). Whether eCBs impact the formation of the endocrine pancreas and predispose it to long-lasting changes in hormone release postnatally remains unknown.

Because eCBs broadly affect cell proliferation, fate, motility, and differentiation (e.g., in sperm, hematopoietic and T cells, and neurons) (10–13), it is likely that they play a role in the cellular organization of developing pancreatic islets, possibly by affecting the spatial segregation of α and β cells. A contribution of eCBs to cell diversification and positioning in the developing pancreas is supported by the temporal control of their levels in fetal tissues (14) and circulation (15). Moreover, α and β cells in mature pancreatic islets express the molecular machinery for eCB metabolism together with CB_1Rs and transient receptor potential cation channels, particularly subfamily V member 1 (TRPV1) (2, 16, 17). Understanding these developmental processes is also relevant to postnatal life because pancreatic α- and β-cell placement can be reconfigured upon metabolic demands in both rodents (18) and humans (19), altering the efficacy of endocrine responsiveness.

Differential ligand and receptor recruitment within pleiotropic eCB signaling networks might facilitate a cellular context- and stage-dependent diversification of eCB signals. Thus, the coordinated availability of 2-AG and AEA and their varied action on CB_1Rs (20) and TRPV1 channels (21) are well-positioned to orchestrate progenitor proliferation and the survival, migration, and ability of hormone secretion from ensuing differentiated cell lineages. Here, we demonstrate that paracrine 2-AG signaling determines cell segregation via CB_1R-mediated adhesion signaling in the fetal mouse pancreas. In turn, chemical or genetic inactivation of TRPV1s on β cells increases cell proliferation both in vitro and in vivo, typically affecting the size of islets formed. Reducing eCB precursor bioavailability during pregnancy by ω-3 polyunsaturated fatty acid (PUFA) intake increases cellular heterogeneity and improves the temporal coordination of glucagon/insulin release, phenocopying $CB_1R^{-/-}$ mice, as well as human islets (19). Cumulatively, our results outline a candidate mechanism for life-long cellular adaptation to metabolic challenges.

Results

Paracrine 2-AG Axis in the Fetal Pancreas. It is critical to document the cellular sites of eCB metabolism and receptor-mediated signaling to appreciate the abundance, cellular specificity, and modes of communication for these signaling lipids during the

Significance

Glucagon and insulin are produced in distinct cell populations within pancreatic Langerhans islets, where intercellular interactions control their production and release. Modifications to the microstructure of pancreatic islets are implicated in disease pathogenesis, but the developmental rules underlying cell commitment and segregation are incompletely understood. We show that endocannabinoids (ω-6) via CB_1 cannabinoid receptors and endovanilloid ligands via transient receptor potential cation channel subfamily V member 1, as well as dietary ω-3 polyunsaturated fatty acids, affect the cellular organization of pancreatic islets during organ development. Thus, lipid signaling emerges as a key determinant of tissue organization and can program hormone secretion for life.

Author contributions: V.D.M., T.G.M.H., A.D., and T.H. designed research; K. Malenczyk, E.K., F.P., D.C., and P.B. performed research; P.B. and K. Mackie contributed new reagents/analytic tools; K. Malenczyk, E.K., F.P., D.C., and T.H. analyzed data; and K. Malenczyk, V.D.M., T.G.M.H., and T.H. wrote the paper.

Reviewers included: L.G., Lund University; T.L.H., Yale University School of Medicine; and G.K., National Institutes of Health.

The authors declare no conflict of interest.

[1]To whom correspondence may be addressed. Email: tibor.harkany@meduniwien.ac.at or tomas.hokfelt@ki.se.

This article contains supporting information online at www.pnas.org/lookup/suppl/doi:10.1073/pnas.1519040112/-/DCSupplemental.

formation of the endocrine pancreas, even more so because eCB signaling so far has been documented only in the fetal brain and musculature (10, 22) and has been shown to progress from a predominantly autocrine (prenatal) toward a paracrine (postnatal) mode of action (23). Similar changes in the molecular configuration of eCB signaling in the fetal pancreas would have a notable impact on both reconstructing signaling events and interpreting functional outcome and disease relevance.

We used multiple immunofluorescence histochemistry to simultaneously detect CB_1Rs and TRPV1s as eCB-sensing receptors (20, 21), as well as *sn*-1-diacylglycerol lipase α (DAGLα), monoacylglycerol lipase (MAGL), and α/β hydrolase domain-containing 6 serine hydrolase (ABHD6) (24) (defining minimal machinery for 2-AG metabolism), in mice at embryonic day (E) 16.5 (Fig. 1 *A–D1*), at birth, and in adulthood (Fig. S1 and Tables S1 and S2). We refrained from dissecting the anatomy of AEA signaling because its biosynthetic machinery is incompletely understood (25), precluding reliable microscale reconstruction. β, but not α, cells were CB_1R-positive ($^+$) at all developmental stages ($P < 0.003$ for all ranked data β vs. α cells) (Fig. 1 *A–A2* and *E* and Fig. S1 *A–B2*). In contrast, TRPV1 was present in both β and α cells at similar levels during pancreas development, as well as at maturity (Fig. 1 *B–B2* and *F* and Fig. S1 *C–E2*).

We found DAGLα preferentially expressed in α cells of the pancreatic primordium at E16.5 ($P < 0.05$ vs. β cells) (Fig. 1 *C–C2* and *G*), with its levels up-regulated in β cells at birth and throughout adulthood (Fig. S1 *F–G2*). MAGL expression was localized to α cells at all ages tested (Fig. 1 *D* and *H* and Fig. S1 *H, H1,* and *J–J3*). Conversely, ABHD6 immunoreactivity in β cells exceeded that seen in α cells at all ages (Fig. 1 *D1* and *I* and Fig. S1 *I, I1,* and *K–K3*). These data suggest that 2-AG signaling is paracrine first, with α cells being the source and β cells the sensors of 2-AG action (Fig. S1 *L* and *M*). These results are compatible with the hypothesis that intercellular signaling modulates cell identity, mass, and migration during islet formation. In turn, mixed autocrine/paracrine signaling might be favored for cell survival.

Laboratory rodents present core-mantle islet morphology with an α cell mantle enwrapping its β cell-dense core (18). In contrast, the organization of α and β cells in adult human pancreatic islets is remarkably different (Fig. 1*J* and *SI Discussion*) because these cell types remain predominantly interspersed (19). This cellular configuration might be favored upon metabolic challenge because it

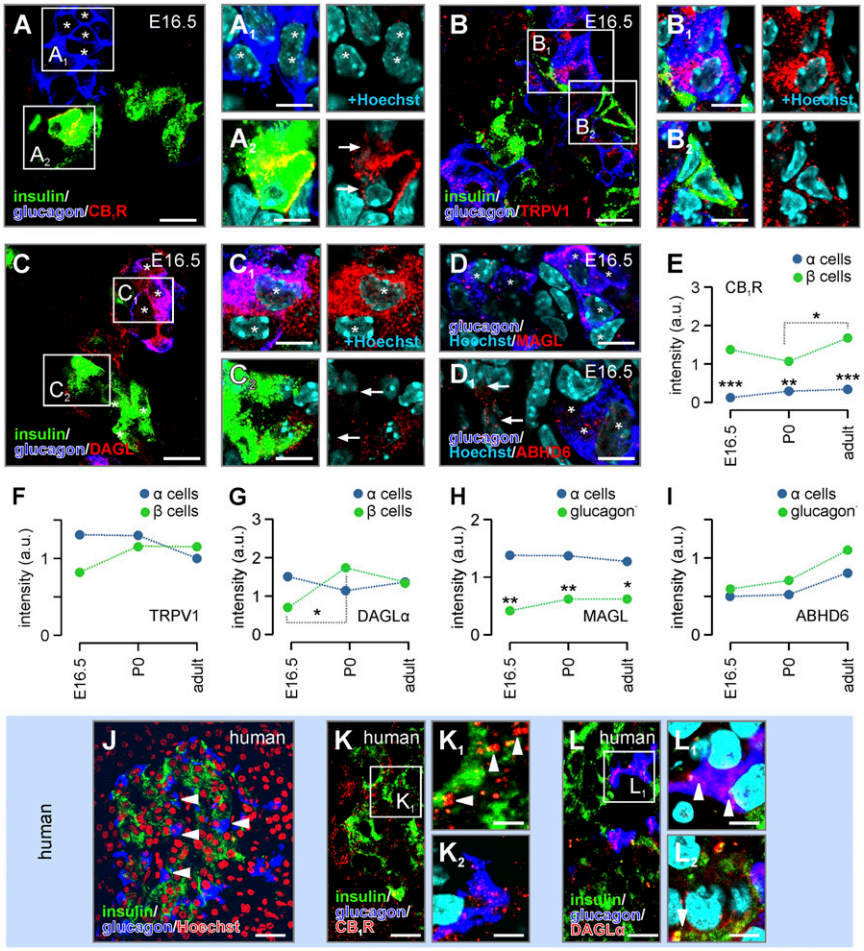

Fig. 1. Spatial segregation of CB_1R and DAGLα in the fetal endocrine pancreas. (*A–A2*) CB_1R immunoreactivity was seen in insulin$^+$/β cells (arrows) but not in glucagon$^+$/α cells (asterisks) at E16.5. (*B–B2*) TRPV1 immunosignals were found in both glucagon$^+$/α cells and insulin$^+$/β cells. (*C–C2*) In contrast, glucagon$^+$/α cells (asterisks) were the primary sites of DAGLα expression at this developmental stage. (*D*) Likewise, MAGL was predominantly localized to glucagon$^+$/α cells (*asterisks*). (*D1*) ABHD6 immunoreactivity localized to both glucagon$^+$/α (asterisks) and glucagon$^-$ cells (arrows). Rectangles indicate the position of *Insets*. Histochemical data from newborn and adult mice are shown in Fig. S2. (*E* and *F–I*) Semiquantitative analysis of CB_1R, TRPV1, DAGLα, MAGL, and ABHD6 immunosignals at successive developmental stages. Statistical comparisons were performed by nonparametric Wilcoxon's rank-sum test, $n = 10$ clusters or islets per group. Data are expressed as medians; $^{***}P < 0.001$, $^{**}P < 0.01$, $^{*}P < 0.05$. (*J–L2*) Glucagon$^+$/α and insulin$^+$/β cell distribution in human pancreatic islets. (*J*) Note that glucagon$^+$/α cells are positioned in pancreatic islet core (arrowheads). CB_1R (*K–K2*) and DAGLα immunosignals (*L–L2*) predominated in insulin$^+$/β cells (arrowheads) and glucagon$^+$/α cells, respectively. Hoechst 33342 was used as nuclear counterstain. (Scale bars: J, 25 μm; *A, B, C, K,* and *L*, 10 μm; *A1, A2, B1, B2, C1, C2, D, D1, K1, K2, L1,* and *L2*, 5 μm.)

could allow the improved coordination of insulin and glucagon release (26). Nevertheless, CB_1R and DAGLα distribution seem evolutionarily conserved and unrelated to cell positioning, inasmuch as CB_1R and DAGLα strictly preferred β and α cells (Fig. 1 *K–L2*), respectively, even if at variable levels in the human biopsies available to us (*SI Discussion*).

Genetic Disruption of 2-AG Signaling Impairs Cell Segregation in Pancreatic Islets. If 2-AG signaling is significant in modulating pancreatic islet microstructure (that is, either the size of α and β cell pools or their spatial positions), then genetic disruption of 2-AG metabolism might impose permanent phenotypes. We have previously found that MAGL-mediated degradation is rate-limiting for fetal 2-AG signaling in brain (23). Therefore, we first tested the analogous hypothesis by determining pancreatic islet morphology in adult $MAGL^{-/-}$ mice. Although the size of pancreatic islets remained unchanged (Fig. 2 *A–B*), $MAGL^{-/-}$ mice showed significantly increased α cell numbers per islet [47 ± 14 ($MAGL^{-/-}$) vs. 22 ± 12 ($MAGL^{+/+}$) cells per section; $P < 0.01$] (Fig. 2*C*). Because the number of β cells was unchanged (Fig. 2*C1*), the calculated α/β cell ratio increased [0.78 ± 0.14 ($MAGL^{-/-}$) vs. 0.29 ± 0.10 ($MAGL^{+/+}$), $P < 0.001$] (Fig. 2*C2*). Significantly, α cells were scattered within islet cores in $MAGL^{-/-}$ mice [0.34 ± 0.07 ($MGL^{-/-}$) vs. 0.14 ± 0.13 ($MAGL^{+/+}$), $P < 0.01$, α cells in core per all α cells] (Fig. 2*D*).

MAGL ablation-induced increased α cell mass and displacement can be due to the transdifferentiation, altered migration, survival, or proliferation of α cell precursors. Therefore, we mapped, in $MAGL^{-/-}$ islets, the expression of Pdx1 and MafA transcription factors that define β cell identity (27) and excluded their presence in glucagon$^+$ α cells (Fig. 2 *A* and *A1*, *Insets* and Fig. S2 *A–B2*). This observation argues against transdifferentiation as a mechanism eliciting altered islet architecture in $MAGL^{-/-}$ mice. Because eCBs modulate cell migration and survival in the nervous system, adipose tissue, muscle, and immune system (13, 22, 28–32), we instead favor that altered cell migration could, at least in part, contribute to incomplete cell segregation in $MAGL^{-/-}$ mice (Fig. S3). Loss of CB_1R function due to receptor desensitization, characterized as CB_1R pools being present intracellularly in $MAGL^{-/-}$ pancreas (Fig. S2 *C* and *D*), supports this hypothesis. Furthermore, the presence of the small GTPase Rac1 (Fig. S4 *A–C1*) and the microtubule-associated protein doublecortin (Fig. S4 *D–I1*) in β and α cells (33) presents downstream targets linked to cytoskeletal reorganization during cell migration (34, 35). These findings are

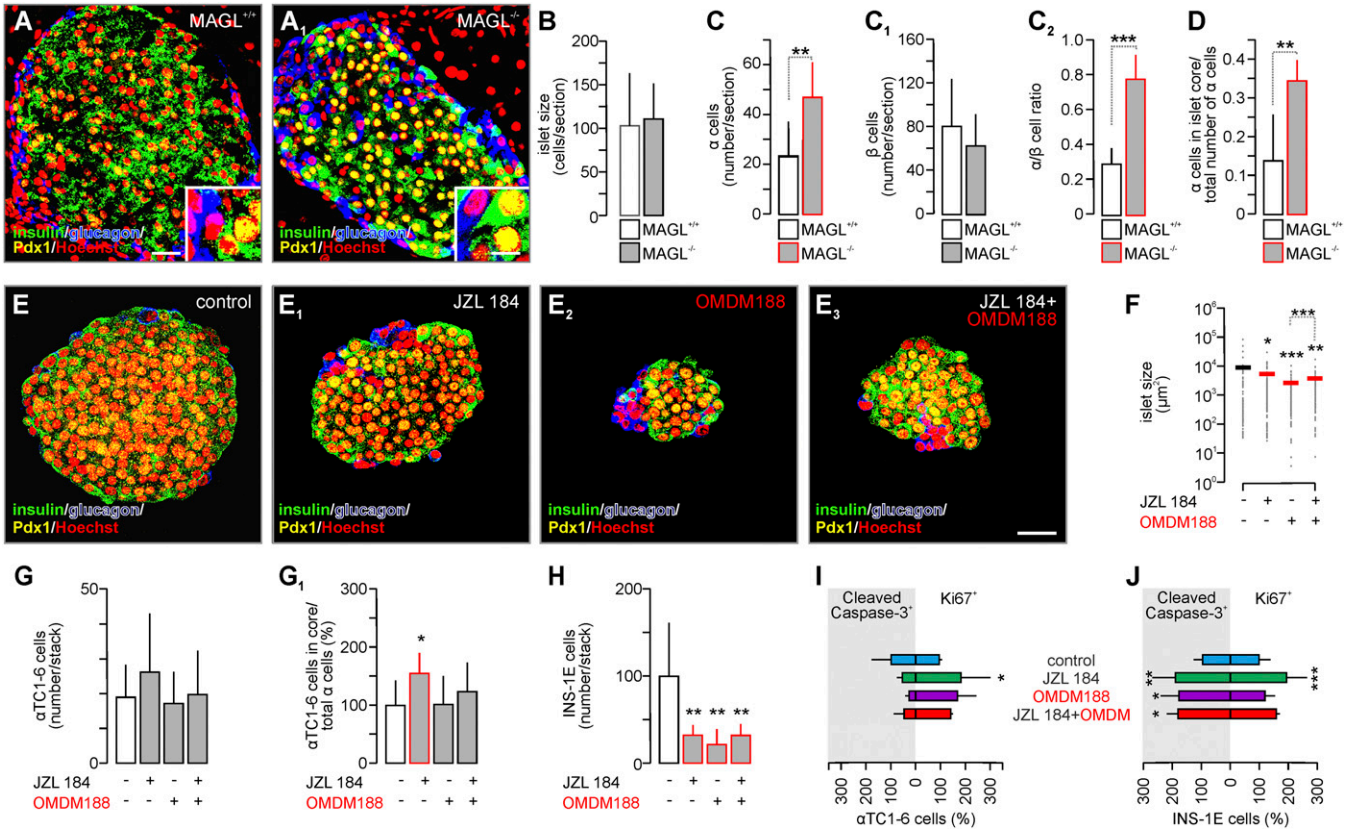

Fig. 2. The cellular organization of pancreatic islets is controlled by 2-AG signaling. (*A* and *A1*) Glucagon$^+$/α and insulin$^+$/Pdx1$^+$/β cell distribution in pancreatic islets from adult $MAGL^{-/-}$ mice relative to WT littermates. Quantitative analysis was performed in $n \geq 3$ animals per genotype. (*B*) Genetic disruption of MAGL did not affect pancreatic islet size. (*C* and *C1*) However, pancreatic islets from $MAGL^{-/-}$ mice contained significantly more α cells whereas the number of β cells remained unchanged. (*C2*) Thus, the ratio of α/β cells significantly increased in pancreatic islets from $MAGL^{-/-}$ mice. (*D*) Genetic manipulation induced incomplete α/β cell segregation with α cells seen in pancreatic islet cores. (*E–E3*) JZL184, an MAGL inhibitor that significantly increases extracellular 2-AG availability (2), as well as OMDM188, a DAGL inhibitor (39), reduced pseudoislet assembly. Hoechst 33342 was used as nuclear counterstain (pseudocolored in red). (Scale bars: 25 μm; *Insets*, 5 μm.) (*F*) Both JZL184 and OMDM188 alone or in combination significantly reduced the size of pseudoislets. (*G*) Neither treatment affected the number of CB_1R^- αTC1-6 cells. Nevertheless, JZL184 induced significant αTC1-6 spread into the pseudoislets' core (*G1*). (*H*) Both JZL184 and OMDM188 significantly reduced the number of INS-1E/β cells in pseudoislets. (*I* and *J*) The rate of apoptosis and cell proliferation, measured by cleaved caspase-3 and Ki67 immunoreactivity, respectively, in αTC1-6 and INS-1E cells cocultured in vitro. Representative images are shown in Fig. S7. (*I*) JZL184 but not OMDM188 increased αTC1-6 cell proliferation and decreased the rate of cell death. (*J*) Quantitative analysis of the rate of apoptosis and proliferation in INS-1E cells revealed increased cell turnover by JZL184. OMDM188 alone or in combination with JZL184 significantly augmented the number of apoptotic INS-1E cells. Data are expressed as means ± SD; $n = 30$ islets per genotype (*B–D*), $n \geq 100$ islets per group (*F*), $n = 10$ islets per group (*G–H*), $n \geq 300$ cells per group (*I* and *J*) were analyzed in triplicate experiments, $^{***}P < 0.001$, $^{**}P < 0.01$, $^{*}P < 0.05$ [Student's *t* test (*B–D*) or post hoc pairwise comparisons, one-way ANOVA].

significant because both Rac1 and doublecortin expressions remain cell type-specific (Fig. S4 *D–I*) and endure into adulthood.

2-AG Signaling Modulates β Cell Survival in Pancreatic Pseudobodies in Vitro. Next, we tested 2-AG's effects on cell aggregation and survival in a model of ordered two-cell clustering (36) amenable to the in vitro chemical probing of signal transduction. αTC1-6 ("α-like") and INS-1E ("β-like") cells were mixed in suspension, producing ordered pseudobodies ("pseudoislets"), which resemble the murine pancreatic islet with an αTC1-6 cell mantle encapsulating a core made up of INS-1E cells (Movie S1). Although αTC1-6 and INS-1E cells are of mouse and rat origins, respectively, and their immortalized nature cautions data interpretation, they are still amenable for our purposes because (*i*) αTC1-6 cells express DAGLα but not CB_1Rs, thus resembling α cells in vivo (Fig. S5); (*ii*) αTC1-6 cells contain and release significantly more 2-AG and AEA than INS-1E, recapitulating in vivo data on α cells being the primary source of eCBs (Fig. S5 *E* and *E1*); (*iii*) neither cell type transdifferentiates when mixed in vitro (Fig. 2 *E–E3*); (*iv*) αTC1-6 cells form spatially ordered 3D-aggregates with INS-1E cells restricted to the core of the pseudoislets (Fig. S6 *A* and *B*); (*v*) both cell lines express vinculin, suggestive of adhesion signaling (Fig. S6*C*) (37); and (*vi*) both retain either glucagon$^+$ or insulin$^+$ and differential responsiveness to glucose when aggregated (Fig. S6 *D* and *E*).

Initially, we assayed whether pharmacological enhancement of 2-AG bioavailability (MAGL inhibition by JZL184, 200 nM) (38) or reduced 2-AG biosynthesis [DAGL inhibition by OMDM188 (100 nM)] (39) affected αTC1-6 and INS-1E interactions. JZL184 moderately, yet significantly, reduced pseudoislet size [6,335 ± 493 (JZL184) vs. 8,731 ± 1,997 μm^2 (control); $F_{(3,815)} = 6.56$, $P < 0.05$]. In contrast, OMDM188 robustly reduced cell clustering (3,976 ± 2,556 μm^2, $P < 0.001$ vs. control) (Fig. 2 *E2* and *F*). JZL184 significantly rescued the OMDM188-induced pseudoislet phenotype [5,697 ± 365 μm^2 (JZL184 + OMDM188) vs. (OMDM188), $P < 0.01$] (Fig. 2 *E3* and *F*).

We then determined whether either treatment modulates α or β cell numbers in individual pseudoislets in vitro. JZL184 did not affect the total number of αTC1-6 cells per pseudoislet (Fig. 2*G*). Nevertheless, JZL184 significantly increased αTC1-6 "mixing," measured as αTC1-6 cells translocated to >10 μm depth from the surface in an OMDM188-sensitive manner [153 ± 35% (JZL184) vs. 100 ± 44% (control); $F_{(3,36)} = 3.25$, $P < 0.05$] (Fig. 2*G1*).

Subsequently, we showed that JZL184 increased αTC1-6 cell proliferation, as measured by Ki67 cytochemistry (40) (Fig. 2*I* and Fig. S7 *A–B3*). For INS-1E cells, DAGL inhibition was detrimental and reduced their numbers [$F_{(3,36)} = 11.82$, e.g., 21 ± 17 (OMDM188) vs. 99 ± 62 cells per cluster (control), $P < 0.01$] (Fig. 2*H*) by promoting apoptosis (Fig. 2*J*). These data suggest that 2-AG signaling is required for pseudoislet assembly and affects their size by limiting the survival of INS-1E cells. Moreover, augmentation of 2-AG signaling for ∼48 h impairs α/β-like cell segregation by misplacement of αTC1-6 cells, corroborating the MAGL$^{-/-}$ phenotype in vivo.

Pseudoislets under control conditions preserved glucose-stimulated insulin (high glucose) and glucagon (low glucose) secretion (Fig. S6 *D* and *E*). As such, JZL184 pretreatment improved both insulin and glucagon release, and significantly increased the insulin-to-glucagon ratio [0.30 ± 0.26 (JZL184) vs. 0.12 ± 0.05 ng/pg (control), $F_{(3,8)} = 4.12$, $P < 0.05$ under peak insulin-permissive conditions] (Fig. S6*F*). This increase was due to the continuously elevated release of insulin upon JZL184 application. In contrast, OMDM188 inhibited glucagon release in 2.75 mM glucose. In sum, 2-AG–induced incomplete cell segregation correlated with improved hormone release.

Altered Adhesion Signaling in MAGL$^{-/-}$ Mice. Tissue architecture relies on how neighboring cells adhere to one another, which is mediated by anchoring systems that link *in trans* elements on partner cells and the extracellular matrix to the cell's cytoskeleton (41). CB_1R inhibition or desensitization disrupts adhesion signaling (2). Here, we tested whether the subcellular distribution of E-cadherin (42) is changed in pancreatic islets of MAGL$^{-/-}$ mice. By quantitative immunofluorescence microscopy, we show that E-cadherin immunoreactivity significantly decreased in adult MAGL$^{-/-}$ β cells [0.75 ± 0.19 (MAGL$^{-/-}$) vs. 1.00 ± 0.29 fold change (MAGL$^{+/+}$), $P < 0.05$] (Fig. 3 *A–D*), which was due to the loss of cytoplasmic E-cadherin [6.81 ± 5.44 (MAGL$^{-/-}$) vs. 32.45 ± 21.14 a.u. (MAGL$^{+/+}$), $P < 0.01$] (Fig. 3*E*). In contrast, E-cadherin levels were significantly increased in MAGL$^{-/-}$ α cells [1.65 ± 0.18 (MAGL$^{-/-}$) vs. 1.00 ± 0.18 fold change (MAGL$^{+/+}$), $P < 0.05$] (Fig. 3 *C–D*), particularly of membranous E-cadherin [91.28 ± 28.16 (MAGL$^{-/-}$) vs. 43.93 ± 22.31 a.u. (MAGL$^{+/+}$), $P < 0.001$] (Fig. 3*F*). These results suggest altered cell–cell contacts as a molecular correlate of incomplete cell segregation.

CB_1Rs Control Cell Sorting in Developing Pancreatic Islets. We hypothesize that eCBs act as positional signals for α and β cells (Fig. S3). However, receptor heterogeneity exists because CB_1R can be coexpressed with TRPV1 receptors in β cells. Therefore, we sought to address the specific contribution of CB_1Rs and TRPV1s to the determination of islet size and cell segregation.

Our above data suggest that 2-AG, which acts at CB_1R but not TRPV1 receptors (43), possibly controls cell sorting in immature pancreatic islets. This notion prompted us to determine whether CB_1R loss of function alters the microarchitecture of mouse pancreatic islets in vivo. The size of pancreatic islets from $CB_1R^{-/-}$ mice remained unchanged (Fig. 4 *A–B* and Fig. S2 *E–F2*). However, we observed an increased number of α cells [38 ± 16 ($CB_1R^{-/-}$) vs. 25 ± 12 ($CB_1R^{+/+}$) cells per section; $P < 0.01$]

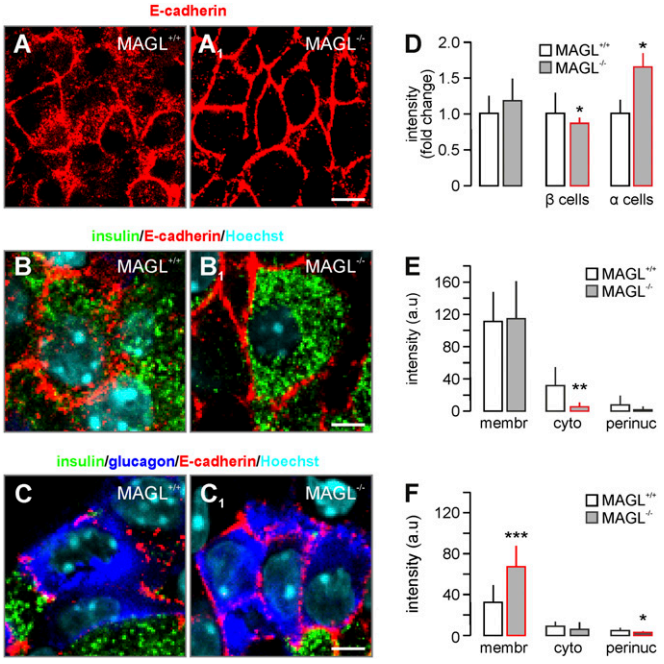

Fig. 3. The 2-AG signals modulate adhesion signaling in pancreatic islets. (*A–C1*) MAGL knockout alters cell adhesion in the adult endocrine pancreas as revealed by E-cadherin immunostaining (*A* and *A1*). E-cadherin immunoreactivity decreased, particularly in the cytoplasm of β cells (*B* and *B1*). In contrast, we found increased membrane-localized E-cadherin in α cells of MAGL$^{-/-}$ mice (*C* and *C1*). Hoechst 33342 was used as nuclear counterstain. (Scale bars: *A* and *A1*, 5 μm; *B–C1*, 2.5 μm.) (*D–F*) Quantitative analysis of the intensity and distribution of E-cadherin immunosignals within pancreatic islets (indiscriminate; *D*), α (*E*), and β cells (*F*) of WT and MAGL$^{-/-}$ mice. Data are expressed as means ± SD; $n = 10$ islets per genotype (*D*), $n = 30$ cells per genotype (*E* and *F*), $n = 10$ islets per group were analyzed in triplicate. ***$P < 0.001$, **$P < 0.01$, *$P < 0.05$ (Student's *t* test). cyto, cytoplasmic; membr, membraneous; perinuc, perinuclear.

(Fig. 4*C*). The number of β cells (Fig. 4*C1*) was unaltered, thus positively skewing the α/β cell ratio [0.48 ± 0.16 ($CB_1R^{-/-}$) vs. 0.33 ± 0.13 ($CB_1R^{+/+}$), $P < 0.001$] (Fig. 4*C2*). Moreover, α cells were scattered within the islet core [0.21 ± 0.07 ($CB_1R^{-/-}$) vs. 0.12 ± 0.08 ($CB_1R^{+/+}$), $P < 0.001$, α cells in core per all α cells] (Fig. 4*D*). These results, and our data from $MAGL^{-/-}$ mice, raise the possibility that disrupted 2-AG signaling impairs cell segregation either due to dysfunctional ($CB_1R^{-/-}$) or desensitized CB_1Rs ($MAGL^{-/-}$ produce chronically and congenitally supraphysiological tissue 2-AG content, which internalizes CB_1Rs in β cells) (Fig. S2 *C* and *D*) (7, 44).

Next, we took advantage of pseudoislets as an in vitro model and used O-2050, a neutral CB_1R antagonist (100 nM) (2), to pharmacologically disrupt CB_1R involvement in α/β cell sorting. O-2050 did not affect pseudoislet size (Fig. 4*E* and Fig. S8 *A* and *A1*), corroborating our in vivo results. Instead, O-2050 significantly increased the number of αTC1-6 cells in pseudoislets [103 ± 43 (O-2050) vs. 17 ± 10 cells per pseudoislet (control), $F_{(3,37)} = 27.04$, $P < 0.001$] (Fig. 4*F*) and their mixing with β cells in pseudoislet cores (Fig. 4*F1*). Subsequently, we exposed pseudoislets to AEA, a mixed eCB/endovanilloid ligand that acts as an agonist at both CB_1Rs and TRPV1s (43). AEA significantly increased pseudoislet diameter [13,789 ± 3,739 μm^2 (AEA) vs. 8,731 ± 1,997 μm^2 (control)] (Fig. 4*E*). AEA not only increased the number of αTC1-6 cells per pseudoislet (32 ± 19) (Fig. 4*F*) but also led to incomplete cell sorting (Fig. 4*F1* and Fig. S8*A2*). Likewise, α and β cell mixing occurred when endogenously produced AEA was tested (URB597; 100 nM) (Fig. S8 *B–B3*). However, AEA did not affect INS-1E cell recruitment to pseudoislets. If dual AEA effects are due to simultaneous signaling at CB_1R and TRPV1 receptors, then coapplied O-2050 can be expected to reveal TRPV1-selective changes. Accordingly, AEA+O-2050 led to the segregation of α- and β-like cells into separate pseudoislets (>40% of pseudoislets contained one predominant cell type) (Fig. S8*A3*). This AEA effect was robust enough to positively bias our size measurements, leading to reduced sizes of single cell type-containing pseudoislets [5,308 ± 360 (AEA + O-2050), $F_{(3,669)} = 6.17$, $P < 0.05$]. Combining AEA and O-2050 reinstated control-equivalent αTC1-6 cell numbers per pseudoislet [18 ± 16 (AEA+O-2050), $P < 0.01$]. Lastly, we observed significant β cell loss upon coapplied AEA and O-2050 [141 ± 57 (AEA) vs. 58 ± 56 (AEA+O-2050), $F_{(3,37)} = 2.84$, $P < 0.05$] (Fig. 4*G*).

αTC1-6 cells do not express appreciable levels of CB_1Rs (Fig. S5). Consequently, O-2050 did not affect either the rate of their proliferation or apoptosis (Fig. 4*H* and Fig. S7 *C–D3*). AEA did not affect αTC1-6 cell proliferation or apoptosis either. In contrast, CB_1R inhibition alone provoked the apoptosis of INS-1E cells [254 ± 26% (O-2050), $F_{(3,10)} = 23.12$, $P < 0.001$], which was not antagonized by AEA coapplication (Fig. 4*I* and Fig. S7 *D–D3*). AEA alone also triggered the apoptosis of INS-1E cells. Neither O-2050 nor AEA affected INS-1E cell proliferation significantly. These data suggest mutually exclusive roles for CB_1R and TRPV1 in determining cellular heterogeneity in pancreatic islets.

TRPV1 Controls Pseudoislet Size. Both native α and β cells express TRPV1 receptors. Our data on AEA suggest that TRPV1 agonism can affect pancreatic islet size. This hypothesis is plausible also because Ca^{2+} signaling (partly through TRPV1) is involved in regulating cell motility and adhesion (42).

To dissect TRPV1 involvement in size determination, we analyzed the morphology of pancreatic islets from $TRPV1^{-/-}$ mice (Fig. 5 *A* and *A1*). Genetic ablation of TRPV1 significantly increased islet size [148 ± 43 ($TRPV1^{-/-}$) vs. 118 ± 44 ($TRPV1^{+/+}$) cells per section, $P < 0.05$] (Fig. 5*B*). The number of α cells did not change significantly. However, we found more β cells in islets from adult $TRPV1^{-/-}$ mice [113 ± 35 ($TRPV1^{-/-}$) vs. 94 ± 30 ($TRPV1^{+/+}$) cells per section, $P < 0.05$] (Fig. 5 *C–C2*). Notably, the relative peripheral position of α cells within the islets was not affected (Fig. 5*D*). Based on these results, we concluded that TRPV1 signaling could regulate the size of, but not cell segregation in pancreatic islets.

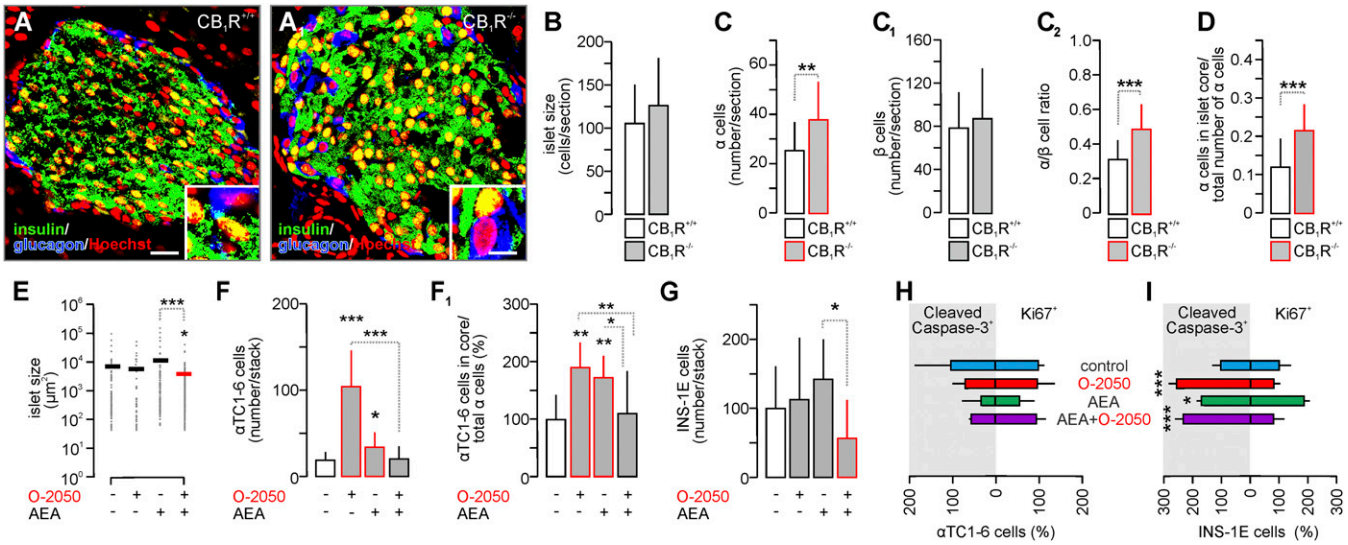

Fig. 4. CB_1R activity orchestrates α and β cell sorting in fetal endocrine pancreas. (*A* and *A1*) Glucagon$^+$/α and insulin$^+$/Pdx1$^+$/β cell distribution in pancreatic islets from adult $CB_1R^{-/-}$ mice relative to WT littermates. Quantitative analysis was performed in $n \geq 3$ animals per genotype. (*B*) Genetic disruption of CB_1R activity did not affect pancreatic islet size. (*C* and *C1*) However, pancreatic islets from $CB_1R^{-/-}$ mice contained significantly more α cells while leaving the β cell pool unchanged. (*C2*) Thus, the ratio of α/β cells significantly increased in pancreatic islets from $CB_1R^{-/-}$ mice. (*D*) Moreover, CB_1R knockout induced incomplete α/β cell segregation with α cells residing in pancreatic islet core. (*E*) AEA increased the size of pseudoislets formed. O-2050 antagonized this effect by sorting αTC1-6 and INS-1E cells to separate clusters. (*F*) AEA and O-2050 increased the number of αTC1-6 cells in individual pseudoislets, including their localization within the pseudoislets' core (*F1*). (*G*) INS-1E cell numbers were not altered by either AEA or O-2050 alone. However, combined treatment led to the formation of small pseudoislets primarily consisting of only one cell type. (*H* and *I*) Quantitative analysis of the rates of apoptosis and proliferation for αTC1-6 and INS-1E cells cultured in the presence of the ligands indicated. Representative images are shown in Fig. S7. Note that CB_1R modulation primarily affected INS-1E cell turnover. Data are expressed as means ± SD; $n = 30$ islets per genotype (*B–D*), $n \geq 100$ islets per group (*E*), $n = 10$ islets per group (*F–G*), $n \geq 300$ cells per group (*H* and *I*) were analyzed in triplicate experiments, $^{***}P < 0.001$, $^{**}P < 0.01$, $^{*}P < 0.05$ [Student's *t* test (*B–D*) or pairwise comparisons/one-way ANOVA].

We confirmed that TRPV1 activation is adverse for pseudoislet formation by using capsaicin (300 nM), a TRPV1 agonist [3,128 ± 654 (capsaicin) vs. 8,731 ± 1,997 μm^2 (control), $F_{(3,184)} = 26.67$, $P < 0.001$] (Fig. 5*E* and Fig. S8 *C* and *C1*). Conversely, capsazepine (10 μM), a TRPV1 antagonist (45), significantly increased the size of the pseudoislets (38,423 ± 4,370, $P < 0.001$) (Fig. 5*E* and Fig. S8 *C* and *C2*). Next, we confirmed these data using AMG 9810, an alternative TRPV1 antagonist (Fig. S8 *D–D3*), which also occluded the effect of capsaicin. Moreover, AEA at the concentration tested did not affect capsazepine (or AMG 9810) effects on islet size [50,751 ± 9,943 μm^2 (AEA + capsazepine), $P < 0.001$ vs. control] (Fig. 5*E* and Fig. S8 *C* and *C3*) but induced significant recruitment [61 ± 53 (AEA + capsazepine) vs. 17 ± 10 cells (control), $F_{(3,36)} = 3.61$, $P < 0.05$] (Fig. 5*F*) and mixing of αTC1-6 cells [185 ± 91% (AEA + capsazepine) vs. 100 ± 44% (control), $F_{(3,36)} = 3.75$, $P < 0.05$] (Fig. 5*F1*) in the pseudoislets. These data clearly dissociate CB_1R vs. TRPV1 outcome in the determination of islet microarchitecture.

Because TRPV1 antagonism alone did not affect the number of αTC1-6 cells in enlarged pseudoislets, we reasoned that an increased contingent of β cells might be recruited (or their survival affected). As Fig. 5*G* shows, quantitative morphometry confirmed this hypothesis [26 ± 16 (capsaicin), 171 ± 45 (capsazepine) and 230 ± 113 (AEA + capsazepine) vs. both $P < 0.01$ vs. 99 ± 62 (control) cell number per section, all $F_{(3,36)} = 16.42$, $P < 0.01$ vs. control].

Lastly, we tested whether changes in αTC1-6 and INS-1E cell numbers in the pseudoislets were related to their altered rate of proliferation and/or apoptosis. Capsaicin remained ineffective in both cell types (Fig. 5 *H* and *I*). Inhibition of TRPV1 signaling by capsazepine, however, significantly reduced the number of Ki67$^+$ (proliferating) αTC1-6 cells [59 ± 40% (capsazepine) vs. 100 ± 15% (control), $F_{(3,9)} = 4.77$, $P < 0.05$] (Fig. 5*H* and Fig. S7 *E–E3*) while being ineffective in altering the rate of αTC1-6 apoptosis (Fig. 5*H* and Fig. S7 *F–F3*). Notably, capsazepine also decreased INS-1E cell turnover [that is, a simultaneous decrease of the histological indices of apoptosis $F_{(3,9)} = 31.13$ and proliferation $F_{(3,9)} = 21.43$, both $P < 0.05$] (Fig. 5*I* and Fig. S7 *E–F3*). These data cumulatively suggest that TRPV1 is a key signaling node controlling pancreatic islet size.

Mixed Pancreatic Islets Favor Insulin over Glucagon Secretion. Increased dietary intake of ω-3 fatty acids is generally accepted to promote leanness by increasing adaptive hormone release from the endocrine pancreas (46, 47). eCBs are derived from arachidonic acid (20:4), an ω-6 PUFA. Correspondingly, ω-3 PUFA-enriched diet during pregnancy lowers 2-AG and AEA levels in the fetus (48). ω-3 PUFA intake is also beneficial for insulin secretion and sensitivity (49–51). Here, we hypothesized that lowering eCB levels during pregnancy and lactation might be reflected in a mixed cell-pancreatic phenotype and improved hormonal responses to glucose in the offspring. We administered an ω3-PUFA–enriched diet to dams starting 3 months before pregnancy and through pregnancy and lactation (Fig. S9*A*). Offspring were weaned onto normal laboratory chow and analyzed when reaching adulthood.

Maternal feeding with an ω3-PUFA–enriched diet resulted in reduced AEA levels in the blood of offspring weaned from ω3-fed mothers [5.20 ± 2.96 (ω3-PUFAs) vs. 24.70 ± 5.06 pmol/mg of lipids (control), $P < 0.01$] (Fig. 6*A*). Dietary intake of ω3-PUFAs did not change the size of pancreatic islets (Fig. 6 *B–C*) or the absolute numbers of α or β cells (Fig. 6 *C1* and *C2*). Interestingly, ω3-PUFAs significantly increased the number of α cells scattered in the islet core [0.28 ± 0.13 (ω3-PUFAs) vs. 0.11 ± 0.09 (control), $P < 0.05$] (Fig. 6*C3*). We then confirmed ω3-PUFA involvement by applying docosahexaenoic acid (DHA) (10 μM) to pseudoislets in vitro. DHA increased the size of pseudoislets [180 ± 55 (DHA) vs. 126 ± 29 (control), $P < 0.05$] (Fig. 6 *D–D2*), as well as increased the number of αTC1-6 cells within pseudoislet cores [163 ± 56% (DHA)

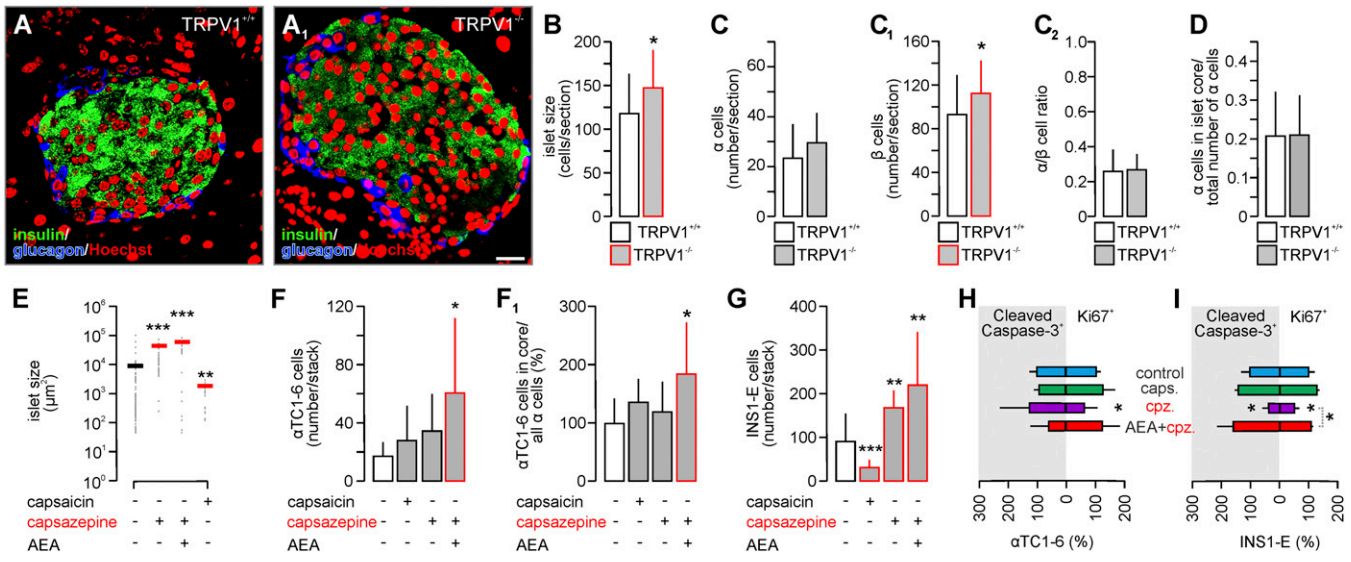

Fig. 5. TPRV1 signaling controls the size of pancreatic islets. (*A* and *A1*) Glucagon$^+$/α and insulin$^+$/β cell distribution in pancreatic islets from adult TRPV1$^{-/-}$ mice relative to WT littermates. Quantitative analysis was performed in $n \geq 3$ animals per genotype. (*B*) Genetic disruption of TRPV1 increased pancreatic islet size. (*C* and *C1*) Although the number of α cells in pancreatic islets from TRPV1$^{-/-}$ mice remained unaffected, they contained significantly more β cells. (*C2* and *D*) Neither the ratio of α/β cells nor their relative positions changed. (*E*) Capsaicin (300 nM, TRPV1 agonist) reduced, whereas capsazepine (cpz) (10 μM, TRPV1 antagonist) increased pseudoislet size. (*F* and *F1*) TRPV1 modulation alone did not affect the number or positioning of αTC1-6 cells. In contrast, AEA (10 μM, endogenous TRPV1 and CB_1R agonist) signaling through cannabinoid receptors in the presence of capsazepine induced αTC1-6 cell recruitment. Thus, AEA distinguished CB_1R and TRPV1-selective mechanisms. (*G*) Capsaicin significantly abrogated whereas capsazepine alone or in combination with AEA increased the number of INS-1E cells. (*H* and *I*) Quantitative assessment of proliferation and apoptosis for αTC1-6 and INS-1E cells. Representative images are shown in Fig. S7. Capsazepine reduced the rate of cell proliferation in both cell lines, as well as reduced INS-1E cell death in vitro. AEA reversed the antiproliferative effect of capsazepine. Hoechst 33342 was used as nuclear counterstain (pseudocolored in red). (Scale bar: 25 μm.) Data are expressed as means ± SD; $n = 20$ islets per group (*B–D*). $n \geq 100$ islets per group (*E*), $n = 10$ pseudoislets per group (*F–G*), $n \geq 300$ cells per group (*H* and *I*) from triplicate experiments, ***$P < 0.001$, **$P < 0.01$, *$P < 0.05$ [pairwise comparisons after one-way ANOVA or Student's *t* test (*B–D*)].

vs. 100 ± 46% (control), $P < 0.05$] (Fig. 6*D3*), recapitulating eCB depletion.

By performing a glucose tolerance test (GTT), we show that blood glucose levels were lower in mice that were characterized by a "mixed" islet phenotype [185.7 ± 28.7 (ω3-PUFA) vs. 231.0 ± 37.5 mg/dL (control), $P < 0.05$, 30 min after glucose injection; area-under-curve, 85 ± 7% of controls] (Fig. 6*E*). In pancreatic islets isolated from these mice, insulin release in response to high glucose was unchanged (Fig. S9*B*). In contrast, glucagon secretion was significantly inhibited in ω3-PUFA–fed mice in response to 2.75 mM glucose (Fig. 6*F*). These changes, when analyzed as an insulin/glucagon ratio, led to a significant shift toward insulin signaling upon stimulation with 16.5 mM glucose [15 min: 0.15 ± 0.03 (ω3-PUFA) vs. 0.08 ± 0.01 ng/pg (control); 20 min: 0.29 ± 0.04 (ω3-PUFA) vs. 0.20 ± 0.05 ng/pg (control), both $P < 0.05$] (Fig. 6*F1*). These data suggest that restricting eCB signaling in utero through dietary modulation of precursor availability might be beneficial for pancreatic functions.

Lastly, we assessed whether morphological phenocopy of pancreatic islets from $CB_1R^{-/-}$ mice produces similar functional outcomes. GTT showed slower decrease in blood glucose in $CB_1R^{-/-}$ mice [218.9 ± 79.3 ($CB_1R^{-/-}$) vs. 145.9 ± 42.0 mg/dL ($CB_1R^{+/+}$), and 174.8 ± 70.1 ($CB_1R^{-/-}$) vs. 116.2 ± 21.1 mg/dL ($CB_1R^{+/+}$), 60 and 90 min after glucose injection respectively, both $P < 0.05$] (Fig. S9*C*). However, $CB_1R^{-/-}$ mice were lean [17.7 ± 2.2 g ($CB_1R^{-/-}$) vs. 20.7 ± 2.3 g ($CB_1R^{+/+}$); $P < 0.05$] (8, 52), expressing lower adipose tissue and muscle to body weight ratio (Fig. S9 *D* and *D1*). These data, supported by an adequate response to insulin [50 ± 8% ($CB_1R^{-/-}$) vs. 54 ± 4% ($CB_1R^{+/+}$) of baseline glucose level 1 h upon insulin challenge], make insulin resistance in $CB_1R^{-/-}$ mice unlikely. Moreover, we observed significant increase in insulin secretion from pancreatic islets isolated from $CB_1R^{-/-}$ in response to 16.5 mM glucose [20 min, 2.36 ± 0.29 ($CB_1R^{-/-}$) vs. 1.37 ± 0.13 ng/mL per islet ($CB_1R^{+/+}$), $P < 0.05$] (Fig. S9*E*) with no change in glucagon secretion (Fig. S9*E1*). This difference manifested as an increased insulin/glucagon ratio upon stimulation with 16.5 mM glucose [15 min, 0.88 ± 0.07 ($CB_1R^{-/-}$) vs. 0.54 ± 0.11 ng/pg ($CB_1R^{+/+}$), $P < 0.05$] (Fig. S9*E2*). Acute CB_1R antagonism reduces insulin release in adult (53). Perinatal CB_1R (in-)activity might instead be beneficial by repositioning cell contingents to improve hormonal coupling. Together, these data suggest that the secretory responsiveness of α and β cells is significantly enhanced by the architectural heterogeneity of pancreatic islets.

Discussion

The present study suggests that paracrine eCB signals are present early in pancreas development in vivo. Even though we are aware of potential limitations of constitutive (vs. inducible) knock-out models, their combination with in vitro pharmacology can sufficiently support the differential engagement of CB_1R and/or TPRV1 receptors to determine the pool size and microtopology of α and β cells in pancreatic islets (Fig. S3). CB_1R and TRPV1s are expressed during postnatal life, and the reconfiguration of pancreatic islets is an "on-demand" mechanism driven by metabolic challenges. Thus, tissue-derived and circulating 2-AG and AEA might bring about critically distinct islet phenotypes associated with or predisposing to metabolic hindrances or disease conditions.

Our secretion assays suggest that the microarchitecture of pancreatic islets is a primary determinant of coordinated insulin and glucagon secretion, with mixed islet phenotypes in rodents being superior to the regular "core-mantle" arrangements. This observation is significant because pancreatic islet morphology is evolutionarily varied (18), reflective of the lifestyle, energy expenditure, and body mass of vertebrate species. As such, mixed pancreatic islets are characteristic of humans and nonhuman primates (18, 19) and suggest an evolutionary selection toward an anatomical microstructure that supports the increased dynamics of hormonal responses, especially in the presence of nutrient abundance. In rodents, reorganization of the core-mantle morphology of pancreatic islets, often interpreted as inadequate, might in fact

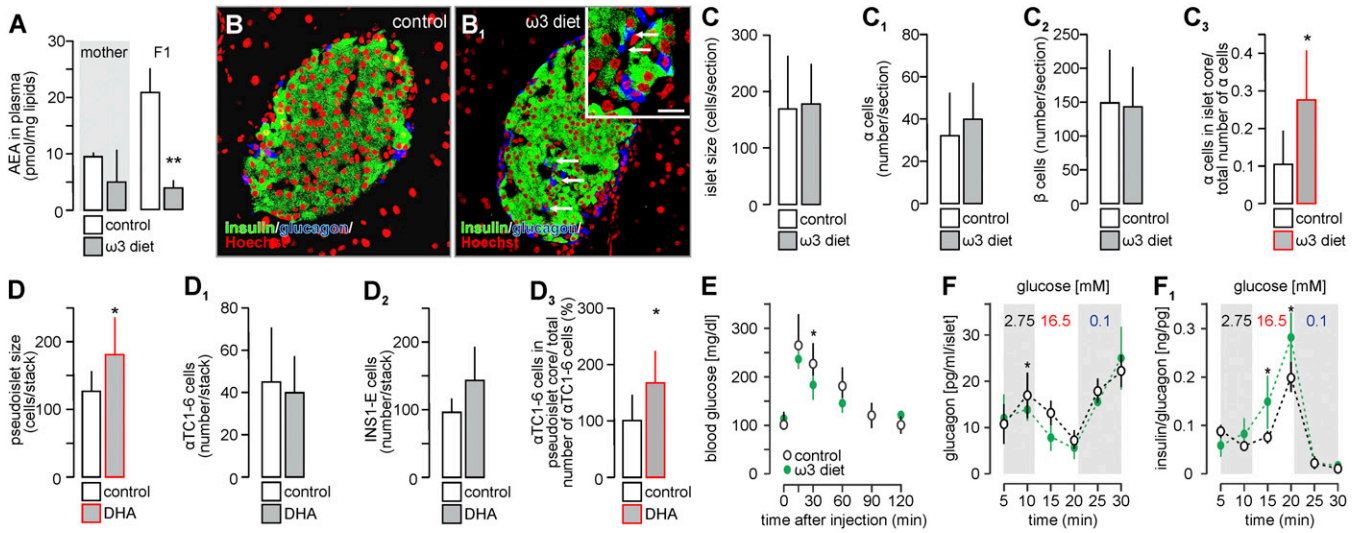

Fig. 6. Incomplete α/β cell sorting leads to improved secretory responses in pancreatic islets. (*A*) ω3 polyunsaturated fatty acid (PUFA)-enriched diet resulted in decreased AEA levels in the blood of offspring as determined by mass spectrometry. (*B* and *B1*) Pancreatic islet morphology in animals fed on normal (*B*) vs. ω3-PUFA–enriched diets until weaning (*B1*). Localization of α cells in ω3-PUFA–fed mice (*Inset*, arrows). Hoechst 33342 was used as nuclear counterstain (pseudocolored in red). (Scale bars: *B1*, 40 μm; *Inset*, 20 μm.) (*C–C3*) Neither the size of individual islets (*C*) nor their α/β cell composition (*C1* and *C2*) was quantitatively altered. Instead, α cells resided in the islet core (>10 μm from the surface; *C3*). (*D–D3*) Quantitative assessment of pseudoislets formed in the presence of docosahexaenoic acid (DHA, 10 μM). DHA increased pseudoislet size (*D*) but not the numbers of αTC1-6 (*D1*) and INS-1E (*D2*) cells forming these clusters. (*D3*) Instead, the number of αTC1-6 cells residing in the psudoislet core was significantly increased. (*E*) Mice prenatally exposed to ω3-PUFAs showed improved glucose tolerance ($n > 6$ per group). (*F*) In primary mouse islets isolated from ω3-PUFA–fed mice, basal release of glucagon was decreased. (*F1*) Moreover, the correlated insulin/glucagon ratio was significantly increased upon high glucose. $n \geq 3$ animals per group were quantitatively assessed. Data are expressed as means ± SD; $n = 30$ islets per group or $n = 10$ pseudoislets per group from triplicate experiments, $^{**}P < 0.01$, $^{*}P < 0.05$ [Student's *t* test (*A–D3*) or pairwise comparisons after one-way ANOVA].

confer adaptation to metabolic or pathogenic challenges. Accordingly, mixed pancreatic islet phenotypes have been associated with both physiological (i.e., pregnancy) (19) and pathophysiological (i.e., obesity, diabetes) (54, 55) conditions impacting glucose sensing and hormone secretion. Thus, we identify eCBs as a signaling network whose ligand diversity in conjunction with the receptor repertoire expressed by α and β cells is poised to tune hormone responsiveness.

eCB signaling has been linked to the molecular control of insulin and glucagon release (2–4). Considering that both $CB_1R^{-/-}$ and $MAGL^{-/-}$ mice are lean (7, 8), we suggest that their mixed pancreatic islets allow for improved short-range insulin signaling between α and β cells ("histoarchitectural gain of function"), which can serve as a feedback mechanism increasing the ratio of insulin to glucagon secretion under high glucose availability. This hypothesis is also supported by genetic data upon conditional insulin receptor knockout in α cells (56), which induces hyperglucagonemia and glucose intolerance. Nevertheless, islet morphologies of adult $CB_1R^{-/-}$ and $MAGL^{-/-}$ mice might represent either the outcome of developmental mechanisms or use-dependent and transient postnatal reorganization. The latter arrangement is particularly relevant in $MAGL^{-/-}$ mice because MAGL deletion affects not only 2-AG contents but also arachidonate precursor pools for prostaglandin synthesis (57), diversifying phenotypic outcome and cellular composition (e.g., macrophage infiltration) (58). Our ω3-PUFA enrichment during embryonic and neonatal development and the ensuing incomplete α/β cell sorting phenotype suggest that reduced eCB bioavailability and signaling in utero (48) generate pancreatic islets mimicking $CB_1R^{-/-}$ or $MAGL^{-/-}$ phenotypes. Implicating eCBs in these processes is appealing because mouse β cells lack GPR120, a "ω3-PUFA receptor" (59) (*SI Discussion*).

AEA and 2-AG exhibit remarkably different receptor specificities: Whereas both 2-AG and AEA bind CB_1/CB_2 cannabinoid receptors, only AEA activates TRPV1 channels (43, 60). We took advantage of this receptor selectivity when combining an in vitro model of ordered α- and β-cell aggregation with mouse genetics. This approach allowed us to dissect the ligand and receptor specificity of eCB signaling in relation to cell sorting and the control of pancreatic pseudoislet size. Thus, CB_1R antagonism by O-2050 or indirectly by inhibiting DAGL-dependent 2-AG biosynthesis increased pseudoislet heterogeneity, identifying CB_1Rs as a critical signaling node for regulating the spatial organization of α and β cells. Notably, OMDM188 eliminated β-cell recruitment to pseudoislets in vitro and enhanced β-cell death whereas both O-2050 and OMDM188 remained ineffective on α-cell proliferation or survival. These results are concordant with our receptor profiling of αTC1-6 and INS-1E cells (2) that suggested the lack of CB_1R expression in αTC1-6 cells. Moreover, pancreatic islet morphology in $MAGL^{-/-}$ and $CB_1R^{-/-}$ mice, where α cells venture extensively into the islet core, supports that both genetic deletion ($CB_1R^{-/-}$) and desensitization ($MAGL^{-/}$) of CB_1Rs (7, 44, 61) inhibit the acquiring of prototypic cellular topography in the murine endocrine pancreas, which we consider as gain of function.

Another key finding of the present report is that TRPV1 agonism decreases whereas antagonism and genetic ablation increase the size of (pseudo)islets (62) without affecting spatial arrangements of α and β cells. Our developmental profiling and in vitro models suggest that TRPV1 signaling in pancreatic islets is independent of pancreatic innervation and relies on AEA as endogenous ligand. Chemical probing of TRPV1s selectively affected β-cell recruitment, and TRPV1 antagonism slowed cell proliferation. Therefore, we hypothesize that TRPV1 signaling is particularly efficacious to regulate the formation of cell–cell contacts underpinning cell aggregation. This finding is not entirely unexpected because previous data implicate signaling at TRPV1s in the proliferation of neural precursors, adipocytes, smooth muscle cells, and keratinocytes (63–66). In addition, the mobilization and aggregation of α and β cells is Ca^{2+}-dependent (42), consistent with a TRPV1-mediated Ca^{2+} influx in pancreatic β cells (45). Therefore, it is tempting to speculate that activation of ligand- or voltage-gated Ca^{2+}-permeable channels other than TRPV1 would recapitulate this prototypic TRPV1 response and could represent druggable targets to ameliorate β-cell dysfunction in diabetes.

Reorganization of pancreatic islet architecture can result from cell transdifferentiation, altered proliferation, survival, or migration related to remodeled cell–cell contacts (27, 67). Transdifferentiation is unlikely to confound our experiments because both α and β cells retained their lineage identities as suggested by the selective presence of Pdx1 and MafA transcription factors in β cells, and glucagon expression restricted to α cells (27, 68). This observation suggests that an eCB-mediated multicomponent mechanism operates during islet development: (*i*) 2-AG–induced CB_1R activity is a survival signal for β but not α cells and supports the increased α/β cell ratio in (pseudo)islets when CB_1R are inhibited; (*ii*) eCBs control cell turnover of both cell types; this suggestion is not surprising because eCBs regulate the proliferation of neural progenitors, adipocytes, and myoblasts (22, 69, 70); and (*iii*) eCBs affect cell motility and adhesion signaling.

We suggest that 2-AG signals can reorganize subcellular E-cadherin localization, with opposite outcomes in α and β cells. We propose that increased E-cadherin expression in α cells dispersed in islet cores is for the ectopic anchoring of resident β cells (67), and allows *in trans* signaling for coordinated hormone secretion. Our E-cadherin data also support the hypothesis that active cell migration participates in mixed islet configuration (67). As such, CB_1R activation by both eCBs and synthetic agonists promotes the long-distance migration of neuroblasts and endothelial cells (29, 30). Moreover, CB_1Rs can signal through small GTPases, including RhoA and Rac1 in neurons (10), thus critically tuning cytoskeletal instability during neuronal morphogenesis and polarization. Our finding that Rac1 is expressed by both α and β cells and that Rac1 is crucial for pancreatic morphogenesis (35) identifies cell migration as a candidate mechanism for core-mantle cell sorting. This notion is further underscored by high doublecortin expression in α cells scattered in islet cores because doublecortin is a ubiquitous marker of cell motility during fetal organogenesis.

The endocrine pancreas is indispensable for adequately orchestrated insulin and glucagon release to maintain the body's energy homeostasis (1, 71) and to protect it from noxious metabolic stress (72–74). Our knockout analysis focused on adult animals because both $CB_1R^{-/-}$ and $MAGL^{-/-}$ mice are lean (7, 8, 52) and resistant to high-fat diet-induced obesity or diabetes (4, 7–9). Although unchanged basal blood glucose and insulin levels of $CB_1R^{-/-}$ and $MAGL^{-/-}$ mice were reported under standard feeding conditions (7, 52), glucagon regulation—and particularly insulin/glucagon balance—in these mice remain unknown. We demonstrate slowed glucose clearance in young $CB_1R^{-/-}$ mice, which is corroborated by recent data (9). Our mechanistic analysis suggests that this profile rather reflects the decreased glucose need of peripheral tissues than any metabolic impairment because (*i*) both fasting (baseline) and terminal glucose levels are unchanged, (*ii*) $CB_1R^{-/-}$ mice exhibit reduced muscle and adipose tissue mass (8), (*iii*) $CB_1R^{-/-}$ mice respond properly to insulin challenge, and (*iv*) in islets isolated from $CB_1R^{-/-}$ mice when islet dissection precludes the influence of tissue-derived or environmental confounds on glucose utilization, an improved relationship of insulin and glucagon secretion was observed. Likewise, we found improved insulin vs. glucagon secretion from morphologically similar pancreatic islets isolated from mice subjected to ω3-PUFA enrichment during fetal development. These data cumulatively link α cells infiltrating the core of pancreatic islets to enhanced α/β cell interplay and hormonal responsiveness. Therefore, we formulate the hypothesis that the increased number of α and β cell contacts drives paracrine signaling in the endocrine pancreas (19, 73), possibly with insulin and glucagon secretion serving as a dual feedback mechanism for α and β cells, respectively (56, 75, 76).

In conclusion, our report identifies fundamental roles for eCBs acting at CB_1R and TRPVs in determining cellular diversity, structural complexity, and life-long plasticity of the endocrine pancreas.

We also highlight that maternal dietary choices during pregnancy can program fetal pancreas development by altering eCB bioavailability (48, 77), which prospectively determines the offspring's sensitivity to metabolic stressors. This observation has clinicopathological significance by pointing to an increased risk of diabetes in either malnourished or obese mothers and underpins the clinical potential of tissue-selective regulation of eCB levels.

Experimental Procedures

Formation of α/β Cell Clusters, "Pseudoislets," in Vitro. INS-1E and αTC1-6 were cocultured at a 2:1 ratio in hybrid medium (10 mL) in 125-mL Erlenmeyer flasks under continuous agitation on gyrating shakers (70 rpm) at 37 °C for 48 h (36). The microarchitecture of pseudoislets was analyzed by capturing serial orthogonal *z*-image stacks (2.5 μm optical thickness) by laser-scanning microscopy. The density and positions of αTC1-6 and INS1-E cells were calculated using ImageJ v1.45 with appropriate plug-ins. The core of each pseudoislet was defined as its volume >10 μm from the outer surface of the spherical structure.

Prenatal Exposure to ω3-Polyunsaturated Fatty Acid-Enriched Diet. Female C57Bl6/N mice (6 wk of age) were continuously fed with an experimental diet enriched in ω3-polyunsaturated fatty acids (21.42 kJ/g; 35% fat including 23.9% ω3 PUFA in the total diet, 25% crude protein, 40% carbohydrate; Special Diets Services) for 3 months before mating and during pregnancy and lactation. Pups were weaned on P21 and reared on a standard laboratory formulation. Control animals were exposed to a standard chow (energy, 15.38 kJ/g; 10% fat, 20% crude protein, 70% carbohydrate; Special Diets Services). Bodyweight of the offspring was measured every other day. At 6 wk of age, animals ($n = 6$ per group) underwent a glucose tolerance test (GTT) (*SI Experimental Procedures*) followed by the isolation of their pancreatic islets.

Statistics. Experiments were performed in triplicate unless stated otherwise. The Wilcoxon rank-sum test was used to analyze data on expression of the eCB system in pancreas during pre- and postnatal development after semiquantitative assessment with data presented as medians. Data from pharmacology experiments were analyzed using one-way ANOVA followed by pairwise comparisons. Student's *t* test (independent group design) was used to statistically evaluate data on pancreatic islet morphology and architecture in transgenic mice and after ω3-PUFA feeding. Data are expressed as means ± SD unless stated otherwise. Fold changes represent the percentage change from the untreated (control) value in individual experiments. A $P < 0.05$ value was considered statistically significant. A 3D rendering was used to qualitatively highlight cumulative changes in "eCB tone" during pancreas development.

Experiments on live animals conformed to the 86/609/EEC directive and were approved by the regional authority (Stockholm Norra Djuretiska Nämnd; N512/12). Ethical approval for use of human samples (Dnr: 00–128, Dnr 2010–279) was obtained from the Committee of Ethics, Faculty of Medicine, Uppsala University with informed consent from the individuals.

ACKNOWLEDGMENTS. We thank Dr. Benjamin F. Cravatt, Dr. Z. Lele, and the National Institute on Drug Abuse for monoacylglycerol lipase (MAGL), TRPV1, and CB_1R knockout mice, and Dr. C. Wollheim and Dr. H. Mulder for INS-1E and αTC1-6 cells, respectively. We thank the CLICK Imaging Facility at Karolinska Institutet for assistance with image processing. This work was supported by Foundation for Polish Science Grants TEAM/2010–5/2 (to A.D.) and MPD/2009/4 (to A.D.), National Science Center Grant UMO-2011/03/B/NZ4/03055 (to A.D.), National Science Centre Grant UMO-2013/10/E/NZ3/00670 (to A.D.), National Institutes of Health Grants DA023214 (to T.H.), DA011322 (to K. Mackie), and DA021696 (to K. Mackie), the Swedish Research Council (T.H. and T.G.M.H.), Hjärnfonden (T.H.), the Petrus and Augusta Hedlunds Foundation (T.H. and T.G.M.H.), and the Novo Nordisk Foundation (T.H. and T.G.M.H.). The Visby Scholarship Program supported K. Malenczyk's studies in Sweden. D.C. is the recipient of a Karolinska Institutet-National Institutes of Health "Training Program in Neuroscience" grant.

1. Matias I, Di Marzo V (2007) Endocannabinoids and the control of energy balance. *Trends Endocrinol Metab* 18(1):27–37.
2. Malenczyk K, et al. (2013) CB1 cannabinoid receptors couple to focal adhesion kinase to control insulin release. *J Biol Chem* 288(45):32685–32699.
3. Li C, et al. (2011) Cannabinoid receptor agonists and antagonists stimulate insulin secretion from isolated human islets of Langerhans. *Diabetes Obes Metab* 13(10): 903–910.
4. Vilches-Flores A, Hauge-Evans AC, Jones PM, Persaud SJ (2013) Chronic activation of cannabinoid receptors in vitro does not compromise mouse islet function. *Clin Sci (Lond)* 124(7):467–478.
5. Li C, et al. (2012) Expression and function of monoacylglycerol lipase in mouse β-cells and human islets of Langerhans. *Cell Physiol Biochem* 30(2):347–358.
6. Matias I, et al. (2006) Regulation, function, and dysregulation of endocannabinoids in models of adipose and beta-pancreatic cells and in obesity and hyperglycemia. *J Clin Endocrinol Metab* 91(8):3171–3180.
7. Taschler U, et al. (2011) Monoglyceride lipase deficiency in mice impairs lipolysis and attenuates diet-induced insulin resistance. *J Biol Chem* 286(20):17467–17477.
8. Oosterveer MH, et al. (2011) Resistance to diet-induced adiposity in cannabinoid receptor-1 deficient mice is not due to impaired adipocyte function. *Nutr Metab (Lond)* 8:93.
9. Li Z, Schmidt SF, Friedman JM (2013) Developmental role for endocannabinoid signaling in regulating glucose metabolism and growth. *Diabetes* 62(7):2359–2367.
10. Harkany T, et al. (2007) The emerging functions of endocannabinoid signaling during CNS development. *Trends Pharmacol Sci* 28(2):83–92.
11. Lewis SE, et al. (2012) Differences in the endocannabinoid system of sperm from fertile and infertile men. *PLoS One* 7(10):e47704.
12. Patinkin D, Milman G, Breuer A, Fride E, Mechoulam R (2008) Endocannabinoids as positive or negative factors in hematopoietic cell migration and differentiation. *Eur J Pharmacol* 595(1-3):1–6.
13. Lombard C, Hegde VL, Nagarkatti M, Nagarkatti PS (2011) Perinatal exposure to Δ9-tetrahydrocannabinol triggers profound defects in T cell differentiation and function in fetal and postnatal stages of life, including decreased responsiveness to HIV antigens. *J Pharmacol Exp Ther* 339(2):607–617.
14. Berrendero F, Sepe N, Ramos JA, Di Marzo V, Fernández-Ruiz JJ (1999) Analysis of cannabinoid receptor binding and mRNA expression and endogenous cannabinoid contents in the developing rat brain during late gestation and early postnatal period. *Synapse* 33(3):181–191.
15. Brocato B, et al. (2013) Endocannabinoid crosstalk between placenta and maternal fat in a baboon model (Papio spp.) of obesity. *Placenta* 34(11):983–989.
16. Kim W, et al. (2012) Cannabinoids induce pancreatic β-cell death by directly inhibiting insulin receptor activation. *Sci Signal* 5(216):ra23.
17. Starowicz KM, et al. (2008) Endocannabinoid dysregulation in the pancreas and adipose tissue of mice fed with a high-fat diet. *Obesity (Silver Spring)* 16(3):553–565.
18. Steiner DJ, Kim A, Miller K, Hara M (2010) Pancreatic islet plasticity: Interspecies comparison of islet architecture and composition. *Islets* 2(3):135–145.
19. Cabrera O, et al. (2006) The unique cytoarchitecture of human pancreatic islets has implications for islet cell function. *Proc Natl Acad Sci USA* 103(7):2334–2339.
20. Matsuda LA, Lolait SJ, Brownstein MJ, Young AC, Bonner TI (1990) Structure of a cannabinoid receptor and functional expression of the cloned cDNA. *Nature* 346(6284): 561–564.
21. Zygmunt PM, et al. (1999) Vanilloid receptors on sensory nerves mediate the vasodilator action of anandamide. *Nature* 400(6743):452–457.
22. Iannotti FA, et al. (2014) The endocannabinoid 2-AG controls skeletal muscle cell differentiation via CB1 receptor-dependent inhibition of Kv7 channels. *Proc Natl Acad Sci USA* 111(24):E2472–E2481.
23. Keimpema E, et al. (2010) Differential subcellular recruitment of monoacylglycerol lipase generates spatial specificity of 2-arachidonoyl glycerol signaling during axonal pathfinding. *J Neurosci* 30(42):13992–14007.
24. Marrs WR, et al. (2010) The serine hydrolase ABHD6 controls the accumulation and efficacy of 2-AG at cannabinoid receptors. *Nat Neurosci* 13(8):951–957.
25. Okamoto Y, Morishita J, Tsuboi K, Tonai T, Ueda N (2004) Molecular characterization of a phospholipase D generating anandamide and its congeners. *J Biol Chem* 279(7): 5298–5305.
26. Kim A, et al. (2009) Islet architecture: A comparative study. *Islets* 1(2):129–136.
27. Gao T, et al. (2014) Pdx1 maintains β cell identity and function by repressing an α cell program. *Cell Metab* 19(2):259–271.
28. Williams EJ, Walsh FS, Doherty P (2003) The FGF receptor uses the endocannabinoid signaling system to couple to an axonal growth response. *J Cell Biol* 160(4):481–486.
29. Oudin MJ, et al. (2011) Endocannabinoids regulate the migration of subventricular zone-derived neuroblasts in the postnatal brain. *J Neurosci* 31(11):4000–4011.
30. Pisanti S, et al. (2011) Genetic and pharmacologic inactivation of cannabinoid CB1 receptor inhibits angiogenesis. *Blood* 117(20):5541–5550.
31. Sütterlin P, et al. (2013) The molecular basis of the cooperation between EGF, FGF and eCB receptors in the regulation of neural stem cell function. *Mol Cell Neurosci* 52:20–30.
32. Muccioli GG, et al. (2010) The endocannabinoid system links gut microbiota to adipogenesis. *Mol Syst Biol* 6:392.
33. Jiang L, et al. (2013) LC-MS/MS identification of doublecortin as abundant beta cell-selective protein discharged by damaged beta cells in vitro. *J Proteomics* 80:268–280.
34. Gleeson JG, Lin PT, Flanagan LA, Walsh CA (1999) Doublecortin is a microtubule-associated protein and is expressed widely by migrating neurons. *Neuron* 23(2): 257–271.
35. Greiner TU, Kesavan G, Ståhlberg A, Semb H (2009) Rac1 regulates pancreatic islet morphogenesis. *BMC Dev Biol* 9:2.
36. Hamaguchi K, Utsunomiya N, Takaki R, Yoshimatsu H, Sakata T (2003) Cellular interaction between mouse pancreatic alpha-cell and beta-cell lines: Possible contact-dependent inhibition of insulin secretion. *Exp Biol Med (Maywood)* 228(10):1227–1233.
37. Guo J, Liu LJ, Yuan L, Wang N, De W (2011) Expression and localization of paxillin in rat pancreas during development. *World J Gastroenterol* 17(40):4479–4487.
38. Long JZ, et al. (2009) Selective blockade of 2-arachidonoylglycerol hydrolysis produces cannabinoid behavioral effects. *Nat Chem Biol* 5(1):37–44.
39. Ortar G, et al. (2008) Tetrahydrolipstatin analogues as modulators of endocannabinoid 2-arachidonoylglycerol metabolism. *J Med Chem* 51(21):6970–6979.

40. Gerdes J, Schwab U, Lemke H, Stein H (1983) Production of a mouse monoclonal antibody reactive with a human nuclear antigen associated with cell proliferation. *Int J Cancer* 31(1):13–20.
41. Gumbiner BM (1996) Cell adhesion: The molecular basis of tissue architecture and morphogenesis. *Cell* 84(3):345–357.
42. Rouiller DG, Cirulli V, Halban PA (1991) Uvomorulin mediates calcium-dependent aggregation of islet cells, whereas calcium-independent cell adhesion molecules distinguish between islet cell types. *Dev Biol* 148(1):233–242.
43. Pertwee RG (2006) The pharmacology of cannabinoid receptors and their ligands: An overview. *Int J Obes* 30(Suppl 1):S13–S18.
44. Schlosburg JE, et al. (2010) Chronic monoacylglycerol lipase blockade causes functional antagonism of the endocannabinoid system. *Nat Neurosci* 13(9):1113–1119.
45. Fågelskiöld AJ, et al. (2012) Insulin-secreting INS-1E cells express functional TRPV1 channels. *Islets* 4(1):56–63.
46. Albert BB, et al. (2014) Higher omega-3 index is associated with increased insulin sensitivity and more favourable metabolic profile in middle-aged overweight men. *Sci Rep* 4:6697.
47. Adler AI, Boyko EJ, Schraer CD, Murphy NJ (1994) Lower prevalence of impaired glucose tolerance and diabetes associated with daily seal oil or salmon consumption among Alaska Natives. *Diabetes Care* 17(12):1498–1501.
48. D'Asti E, et al. (2010) Maternal dietary fat determines metabolic profile and the magnitude of endocannabinoid inhibition of the stress response in neonatal rat offspring. *Endocrinology* 151(4):1685–1694.
49. Wei D, et al. (2010) Cellular production of n-3 PUFAs and reduction of n-6-to-n-3 ratios in the pancreatic beta-cells and islets enhance insulin secretion and confer protection against cytokine-induced cell death. *Diabetes* 59(2):471–478.
50. Piscitelli F, et al. (2011) Effect of dietary krill oil supplementation on the endocannabinoidome of metabolically relevant tissues from high-fat-fed mice. *Nutr Metab (Lond)* 8(1):51.
51. Batetta B, et al. (2009) Endocannabinoids may mediate the ability of (n-3) fatty acids to reduce ectopic fat and inflammatory mediators in obese Zucker rats. *J Nutr* 139(8): 1495–1501.
52. Ravinet Trillou C, Delgorge C, Menet C, Arnone M, Soubrié P (2004) CB1 cannabinoid receptor knockout in mice leads to leanness, resistance to diet-induced obesity and enhanced leptin sensitivity. *Int J Obes Relat Metab Disord* 28(4):640–648.
53. Getty-Kaushik L, et al. (2009) The CB1 antagonist rimonabant decreases insulin hypersecretion in rat pancreatic islets. *Obesity (Silver Spring)* 17(10):1856–1860.
54. Hart AW, Baeza N, Apelqvist A, Edlund H (2000) Attenuation of FGF signalling in mouse beta-cells leads to diabetes. *Nature* 408(6814):864–868.
55. Mastracci TL, Sussel L (2012) The endocrine pancreas: Insights into development, differentiation, and diabetes. *Wiley Interdiscip Rev Dev Biol* 1(5):609–628.
56. Kawamori D, Kulkarni RN (2009) Insulin modulation of glucagon secretion: The role of insulin and other factors in the regulation of glucagon secretion. *Islets* 1(3): 276–279.
57. Nomura DK, et al. (2011) Endocannabinoid hydrolysis generates brain prostaglandins that promote neuroinflammation. *Science* 334(6057):809–813.
58. Tam J, et al. (2010) Peripheral CB1 cannabinoid receptor blockade improves cardiometabolic risk in mouse models of obesity. *J Clin Invest* 120(8):2953–2966.
59. Oh DY, et al. (2014) A Gpr120-selective agonist improves insulin resistance and chronic inflammation in obese mice. *Nat Med* 20:942–947.
60. Melck D, et al. (1999) Unsaturated long-chain N-acyl-vanillyl-amides (N-AVAMs): Vanilloid receptor ligands that inhibit anandamide-facilitated transport and bind to CB1 cannabinoid receptors. *Biochem Biophys Res Commun* 262(1):275–284.
61. Chanda PK, et al. (2010) Monoacylglycerol lipase activity is a critical modulator of the tone and integrity of the endocannabinoid system. *Mol Pharmacol* 78(6):996–1003.
62. Riera CE, et al. (2014) TRPV1 pain receptors regulate longevity and metabolism by neuropeptide signaling. *Cell* 157(5):1023–1036.
63. Trazzi S, Steger M, Mitrugno VM, Bartesaghi R, Ciani E (2010) CB1 cannabinoid receptors increase neuronal precursor proliferation through AKT/glycogen synthase kinase-3beta/beta-catenin signaling. *J Biol Chem* 285(13):10098–10109.
64. Bellocchio L, Cervino C, Vicennati V, Pasquali R, Pagotto U (2008) Cannabinoid type 1 receptor: Another arrow in the adipocytes' bow. *J Neuroendocrinol* 20(Suppl 1): 130–138.
65. Zhao L, et al. (2013) Effect of TRPV1 channel on the proliferation and apoptosis in asthmatic rat airway smooth muscle cells. *Exp Lung Res* 39(7):283–294.
66. Li S, et al. (2011) TRPV1-antagonist AMG9810 promotes mouse skin tumorigenesis through EGFR/Akt signaling. *Carcinogenesis* 32(5):779–785.
67. Esni F, et al. (1999) Neural cell adhesion molecule (N-CAM) is required for cell type segregation and normal ultrastructure in pancreatic islets. *J Cell Biol* 144(2):325–337.
68. Hang Y, et al. (2014) The MafA transcription factor becomes essential to islet β-cells soon after birth. *Diabetes* 63(6):1994–2005.
69. Aguado T, et al. (2006) The endocannabinoid system promotes astroglial differentiation by acting on neural progenitor cells. *J Neurosci* 26(5):1551–1561.
70. Gary-Bobo M, et al. (2006) The cannabinoid CB1 receptor antagonist rimonabant (SR141716) inhibits cell proliferation and increases markers of adipocyte maturation in cultured mouse 3T3 F442A preadipocytes. *Mol Pharmacol* 69(2):471–478.
71. Unger RH (1981) The milieu interieur and the islets of Langerhans. *Diabetologia* 20(1):1–11.
72. Unger RH, Orci L (1975) The essential role of glucagon in the pathogenesis of diabetes mellitus. *Lancet* 1(7897):14–16.
73. Unger RH, Orci L (2010) Paracrinology of islets and the paracrinopathy of diabetes. *Proc Natl Acad Sci USA* 107(37):16009–16012.
74. Unger RH (2002) Lipotoxic diseases. *Annu Rev Med* 53:319–336.
75. Pipeleers D, in't Veld PI, Maes E, Van De Winkel M (1982) Glucose-induced insulin release depends on functional cooperation between islet cells. *Proc Natl Acad Sci USA* 79(23):7322–7325.
76. Ahrén B, Larsson H (2001) Impaired glucose tolerance (IGT) is associated with reduced insulin-induced suppression of glucagon concentrations. *Diabetologia* 44(11): 1998–2003.
77. Wood JT, et al. (2010) Dietary docosahexaenoic acid supplementation alters select physiological endocannabinoid-system metabolites in brain and plasma. *J Lipid Res* 51(6):1416–1423.
78. Szot GL, Koudria P, Bluestone JA (2007) Murine pancreatic islet isolation. *J Vis Exp* 2007(7):255.
79. Ledent C, et al. (1999) Unresponsiveness to cannabinoids and reduced addictive effects of opiates in CB1 receptor knockout mice. *Science* 283(5400):401–404.
80. Caterina MJ, et al. (2000) Impaired nociception and pain sensation in mice lacking the capsaicin receptor. *Science* 288(5464):306–313.
81. De Marchi N, et al. (2003) Endocannabinoid signalling in the blood of patients with schizophrenia. *Lipids Health Dis* 2:5.
82. Gavva NR, et al. (2005) AMG 9810 [(E)-3-(4-t-butylphenyl)-N-(2,3-dihydrobenzo[b][1,4] dioxin-6-yl)acrylamide], a novel vanilloid receptor 1 (TRPV1) antagonist with antihyperalgesic properties. *J Pharmacol Exp Ther* 313(1):474–484.
83. Fegley D, et al. (2005) Characterization of the fatty acid amide hydrolase inhibitor cyclohexyl carbamic acid 3′-carbamoyl-biphenyl-3-yl ester (URB597): Effects on anandamide and oleoylethanolamide deactivation. *J Pharmacol Exp Ther* 313(1):352–358.
84. Yoshida T, et al. (2006) Localization of diacylglycerol lipase-alpha around postsynaptic spine suggests close proximity between production site of an endocannabinoid, 2-arachidonoyl-glycerol, and presynaptic cannabinoid CB1 receptor. *J Neurosci* 26(18): 4740–4751.
85. Slipetz DM, et al. (1995) Activation of the human peripheral cannabinoid receptor results in inhibition of adenylyl cyclase. *Mol Pharmacol* 48(2):352–361.
86. Mulder J, et al. (2011) Molecular reorganization of endocannabinoid signalling in Alzheimer's disease. *Brain* 134(Pt 4):1041–1060.
87. Rueda-Clausen CF, et al. (2011) Hypoxia-induced intrauterine growth restriction increases the susceptibility of rats to high-fat diet-induced metabolic syndrome. *Diabetes* 60(2):507–516.
88. Ravnskjaer K, et al. (2013) Glucagon regulates gluconeogenesis through KAT2B- and WDR5-mediated epigenetic effects. *J Clin Invest* 123(10):4318–4328.
89. Matsuo K, et al. (2010) Altered glucose homeostasis in mice with liver-specific deletion of Src homology phosphatase 2. *J Biol Chem* 285(51):39750–39758.
90. Kramer B, Buffenstein R (2004) The pancreas of the naked mole-rat (Heterocephalus glaber): An ultrastructural and immunocytochemical study of the endocrine component of thermoneutral and cold acclimated animals. *Gen Comp Endocrinol* 139(3): 206–214.
91. Elphick MR, Egertová M (2001) The neurobiology and evolution of cannabinoid signalling. *Philos Trans R Soc Lond B Biol Sci* 356(1407):381–408.
92. McPartland JM (2004) Phylogenomic and chemotaxonomic analysis of the endocannabinoid system. *Brain Res Brain Res Rev* 45(1):18–29.
93. Jourdan T, et al. (2013) Activation of the Nlrp3 inflammasome in infiltrating macrophages by endocannabinoids mediates beta cell loss in type 2 diabetes. *Nat Med* 19(9):1132–1140.
94. Piomelli D (2003) The molecular logic of endocannabinoid signalling. *Nat Rev Neurosci* 4(11):873–884.
95. Kim HY, et al. (2011) N-Docosahexaenoylethanolamide promotes development of hippocampal neurons. *Biochem J* 435(2):327–336.
96. Kim HY, Spector AA, Xiong ZM (2011) A synaptogenic amide N-docosahexaenoylethanolamide promotes hippocampal development. *Prostaglandins Other Lipid Mediat* 96(1-4):114–120.
97. Kim HY, Spector AA (2013) Synaptamide, endocannabinoid-like derivative of docosahexaenoic acid with cannabinoid-independent function. *Prostaglandins Leukot Essent Fatty Acids* 88(1):121–125.
98. Rashid MA, Katakura M, Kharebava G, Kevala K, Kim HY (2013) N-Docosahexaenoylethanolamine is a potent neurogenic factor for neural stem cell differentiation. *J Neurochem* 125(6):869–884.
99. Zhang D, Leung PS (2014) Potential roles of GPR120 and its agonists in the management of diabetes. *Drug Des Devel Ther* 8:1013–1027.
100. Stone VM, et al. (2014) GPR120 (FFAR4) is preferentially expressed in pancreatic delta cells and regulates somatostatin secretion from murine islets of Langerhans. *Diabetologia* 57(6):1182–1191.
101. Rinaldi-Carmona M, et al. (1994) SR141716A, a potent and selective antagonist of the brain cannabinoid receptor. *FEBS Lett* 350(2-3):240–244.
102. Pavón FJ, et al. (2008) Central versus peripheral antagonism of cannabinoid CB1 receptor in obesity: Effects of LH-21, a peripherally acting neutral cannabinoid receptor antagonist, in Zucker rats. *J Neuroendocrinol* 20(Suppl 1):116–123.
103. Bisogno T, et al. (2003) Cloning of the first sn1-DAG lipases points to the spatial and temporal regulation of endocannabinoid signaling in the brain. *J Cell Biol* 163(3): 463–468.
104. Cravatt BF, et al. (1996) Molecular characterization of an enzyme that degrades neuromodulatory fatty-acid amides. *Nature* 384(6604):83–87.
105. Dinh TP, et al. (2002) Brain monoglyceride lipase participating in endocannabinoid inactivation. *Proc Natl Acad Sci USA* 99(16):10819–10824.
106. Di Marzo V, et al. (1994) Formation and inactivation of endogenous cannabinoid anandamide in central neurons. *Nature* 372(6507):686–691.
107. Baum J, Simons BE, Jr, Unger RH, Madison LL (1962) Localization of glucagon in the alpha cells in the pancreatic islet by immunofluorescent technics. *Diabetes* 11:371–374.
108. Lacy PE, Davies J (1959) Demonstration of insulin in mammalian pancreas by the fluorescent antibody method. *Stain Technol* 34(2):85–89.